Development of an Improved Highway-Vehicle-Object-Simulation Model for Multi-Faced Rigid Barriers

HURON S. PERERA

A new vehicle/barrier crush model was developed to improve the Highway-Vehicle-Object-Simulation Model (HVOSM) to simulate impacts with multi-faced rigid barriers. The crush model accounts for the effects of both the deformation and deformation rate of the vehicle body on the vehicle/barrier interface force. A set of deformation tracking (DT) points was introduced on the vehicle periphery to track the deformation history of the vehicle body during the impact. These points identify the deformation pattern over all contacting surfaces between the vehicle and barrier at each time step. A surface is then fitted to the interface force intensity values at each of these DT points. The sprung-mass-impact-force subroutine of the HVOSM computer program was replaced with a set of subroutines that determine the vehicle/barrier interface force intensity according to the new crush model. Subroutines were also incorporated to integrate the force intensity over the interface area by fitting a surface to the scattered intensity values. Calibration and validation of the program was accomplished by simulating (a) three problems having known solutions, (b) two full-scale crash tests with a rigid wall instrumented to measure the total lateral force on the wall, and (c) seven full-scale crash tests with concrete safety-shape barrier (CSSB). Overall, the program simulated gross vehicle motions for CSSB impacts at an acceptable level of accuracy for a wide range of impact conditions.

Since the early 1960s, the use of concrete safety-shape barriers CSSB on U.S. highways has been increasing. Today, these barriers are deployed along thousands of miles of highway. The CSSB is a rigid barrier that does not deflect to any appreciable degree, even at high dynamic loads. Hence, the CSSB is often the appurtenance chosen for use in construction zones and as bridge rails. For medians along urban freeways with high traffic density, where the probability of a barrier hit is high and the maintenance is difficult, the CSSB is preferred over deformable longitudinal barriers due to its comparatively low maintenance cost. The most common CSSB currently used is the New Jersey profile, which has three sloped faces on either side (see Figure 1).

While the CSSB is recognized as an important development to safely restrain and redirect errant vehicles on the highway, it has the disadvantages of causing high decelerations at high impact angles and vehicle rollover for certain impact conditions. Full-scale crash testing and the simulation by a computer model are the only methods available to investigate these problems. Due to the high costs of full-scale crash tests, they cannot be performed economically to cover the entire set of possible impact conditions. Therefore, developing a simulation tool for vehicular impacts with CSSB is critical.

Texas Transportation Institute, The Texas A&M University System, College Station, Tex. 77843.

The primary objectives of developing such a simulation tool are

- To investigate the performance limit (as measured primarily by vehicle stability and vehicle accelerations) of a particular barrier shape on different vehicle sizes, and
- To compare the performances of various barrier shapes on a given vehicle and under given impact conditions.

The vehicle model chosen for simulation should be capable of simulating three-dimensional vehicular behavior to investigate the effects of different profiles of CSSB on the vehicle's stability. The Highway-Vehicle-Object-Simulation Model (HVOSM) (*1*) has the three translational and three rotational degrees of freedom (DOFs), with four additional DOFs for the relative motion of the suspended wheels and another for steering angle. No other model is able to simulate tires, suspension, and steering behavior to the degree found in HVOSM, therefore, it was chosen for simulation of CSSB impacts.

CRUSHING FORCE AT THE VEHICLE/BARRIER INTERFACE

In the HVOSM, the vehicle sprung mass is treated as a rigid mass surrounded by a layer of isotropic, homogeneous material similar to plastic. The dynamic pressure of the plastic flow process in the peripheral layer of material increases linearly with the depth of penetration, as shown in Figure 2 (*2*). The existing HVOSM program has the capability of simulating a vehicular impact with a vertical wall using this crush model. Vehicle deformations (crush), velocities, accelerations, and crushing forces recorded in a series of frontal crash tests were used to improve this model (*3*). Based on these experimental data, the following crush model was developed and validated. According to this new model, the dynamic pressure (p) at any point of the vehicle/barrier interface is given by

$$p = k_v\delta[1 + c_v(\dot{\delta}/\dot{\delta}_{ref})^{n_v}] \qquad 0 < n_v < 2 \qquad (1)$$

where

δ = the deformation,
$\dot{\delta}$ = the deformation rate,
k_v, c_v and n_v = the constant parameters for a particular vehicle, and
$\dot{\delta}_{ref}$ = a reference velocity term that makes $\dot{\delta}$ dimensionless.

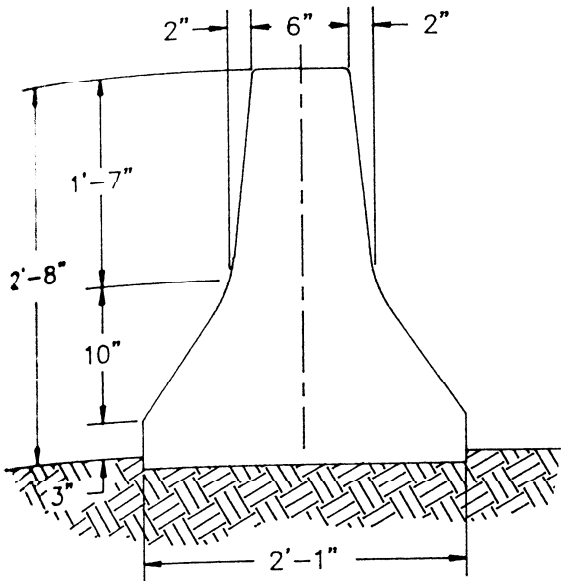

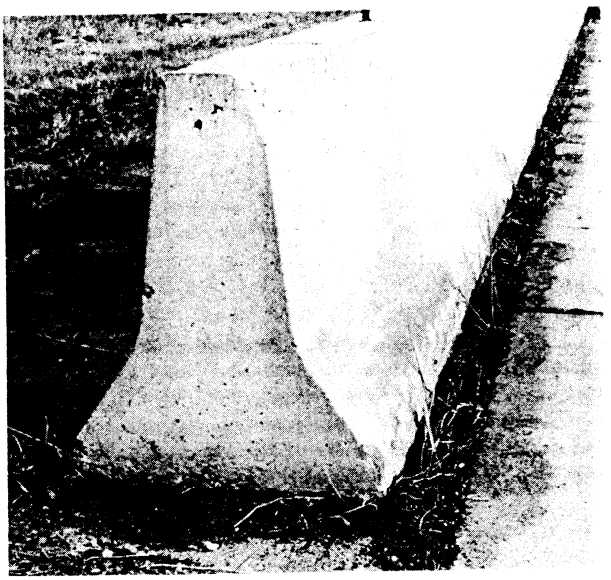

FIGURE 1 Concrete safety-shape barrier with the New Jersey profile.

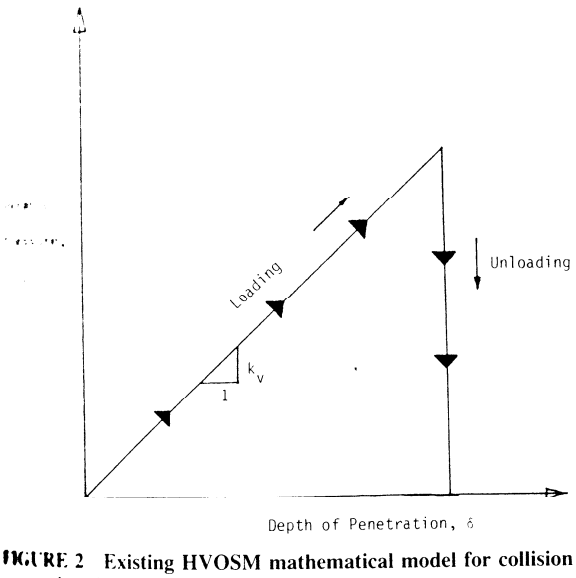

FIGURE 2 Existing HVOSM mathematical model for collision properties of vehicle periphery.

The constant k_v is a force per volume, whereas c_v and n_v are dimensionless. It should be noted that the constant c_v is not a damping coefficient. The reference velocity ($\dot{\delta}_{ref}$) is chosen to be 1 in/sec. In the equations that follow, $\dot{\delta}$ denotes nondimensional velocity, and $\dot{\delta}_{ref}$ does not appear. In an angular impact, both the deformation (δ) and the deformation rate ($\dot{\delta}$) vary over the vehicle/barrier interface. Ranges of k_v, c_v and n_v values for frontal impacts were estimated by simulating 10 frontal crash tests. These are 0.4 through 1.3 kips/in^3 for k_v, 0.004 through 0.04 for c_v, and 0.65 through 1.0 for n_v. An attempt was made to correlate crush parameters k_v, c_v and n_v with the mass of the vehicle. However, a useful relationship could not be found due to scattering of estimated values when plotted against mass m. Lack of data to cover the whole range of vehicle masses from small to large automobiles may have affected the poor correlation of vehicle mass to these parameters.

TRACKING VEHICULAR DEFORMATIONS

According to the crush model given by Equation 1, the normal force on the interface between the kth barrier surface and the vehicle (F_{Nvk}) is given by

$$F_{Nvk} = k_v \int \delta \left[1 + c_v \dot{\delta}^{n_v}\right] dA_{vk} \tag{2}$$

where A_{vk} is the interface area between the vehicle and the kth barrier surface.

The deformation rate ($\dot{\delta}$) at any point on the contact area (A_{vk}) is the velocity of the vehicle at that point, in the direction of the outward normal to the kth barrier surface. This can be easily determined for the given position, orientation, and translational and rotational velocities of the vehicle. However, to find the deformation (δ), the deformation history of each vehicle point on A_{vk} is needed.

To track the deformation history of the vehicle periphery during the crash, a set of points is introduced on the periphery. They are referred to as deformation tracking (DT) points.

Assuming friction between the vehicle and the barrier causes no tangential deformations to the vehicle sheet metal, the DT points will slide along a barrier surface, subject to the friction force. During the rotation of a barrier surface around its axis of rotation within a time step, the surface is assumed to move the DT points it touches in a normal direction. In other words, the points are assumed to move in a circular arc whose center is on the axis of rotation of the barrier surface, as shown in Figure 3. The total deformation of a certain DT point at a certain time is the sum of the lengths of all the circular arcs along which it is moved from the time it started moving.

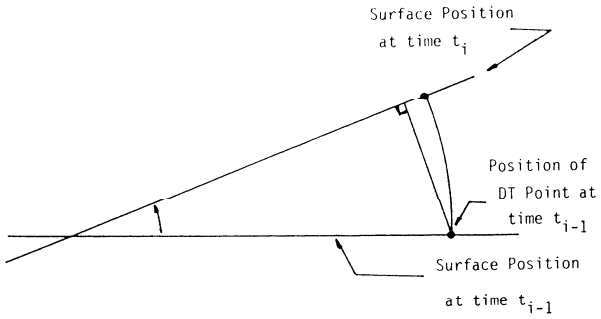

FIGURE 3 Schematic for deformation and positioning of a DT point.

DETERMINATION OF THE VEHICLE/ BARRIER INTERFACE SHAPE

To find the normal forces on the vehicle/barrier surface interfaces, the integration in Equation 2 has to be performed over its region of integration (the contact area between the vehicle and each barrier surface). The existing HVOSM analysis for the simulation of an impact with a vertical wall assumes that the vehicle is a rectangular box; for simplicity of determining the interface polygons, this is assumed in the present analysis also. Therefore, the shape of each vehicle/barrier surface interface is a polygon with sides formed by the upper and lower boundaries of the barrier surface or the intersection of vehicle surfaces with the barrier surface, or both. The procedure used for the determination of corner points of these polygons is described below.

First, the intersection points of the vehicle edges with the plane of the barrier surface are found, assuming that both the vehicle edges and the barrier surface plane are unbounded. Then, the points falling outside the vehicle are rejected. This defines a polygon lying on the unbounded barrier surface plane. Finally, the points falling outside the barrier surface edges are rejected after finding necessary intersections of the polygon's edges with the upper and lower barrier surface edges.

There are two types of vehicle surfaces: the original undeformed vehicle surfaces and the surfaces that are created during the impact by the rotation of the vehicle around a line inside the vehicle/barrier surface contact areas. The latter type are partially deformed. Figure 4 shows a plan view of the vehicle and the possible movements of the kth barrier surface (assumed vertical in the illustration) relative to the vehicle from time t_i to t_{i+1}. These are

a. The vehicle staying in touch with the kth surface, from t_i to t_{i+1};
b. The vehicle leaving the kth surface partially, during the time step; and
c. The vehicle leaving the kth surface fully, during the time step.

It is obvious that cases b and c are creating a partially deformed but currently undeforming vehicle surface. These partially deformed surfaces may take part in forming the corner points of vehicle/barrier surface interfaces for time steps after time t_{i+1}. Therefore, if it is found that any such partially deformed surfaces are formed, then the equations of the vehicle edges formed by the intersection of these planes with the original vehicle surfaces are found, and these new vehicle edges are also considered in the corner point determination of the subsequent time steps.

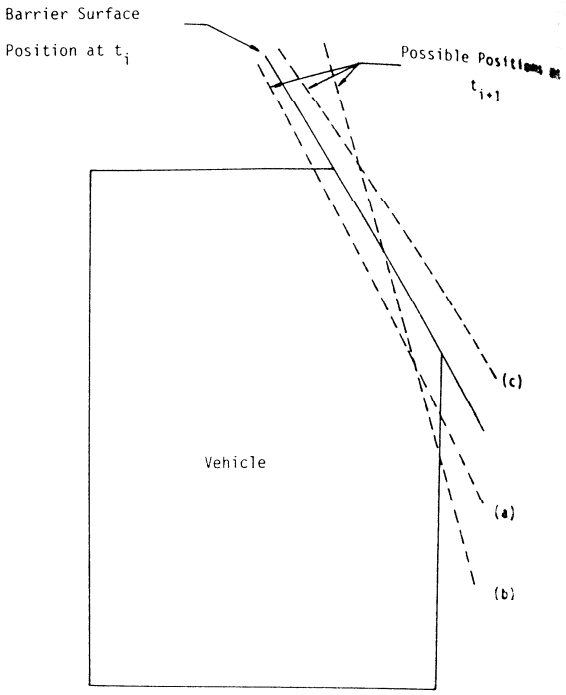

FIGURE 4 Possible movements of a barrier surface with respect to the vehicle during a time step.

DETERMINATION OF THE INTERFACE FORCE

The normal and tangential impact force or moment on the interface between the kth barrier surface and the vehicle are found by integrating force or moment intensities that are functions of deformations δ and deformation rates $\dot{\delta}$ (see Equation 2 for the normal force integral) over interface area A_{sk}. As mentioned earlier, the deformation rate $\dot{\delta}$ at any point on the contact area (needed only at the DT points) is the velocity of the vehicle at that point in the direction of the outward normal to the barrier surface it touches. In addition to this component of the velocity, the direction of the component tangential to the barrier surface is also needed to find the direction of the friction force intensity at that point. Therefore, to find forces or moments on the kth barrier surface, the velocities (components both normal and tangential to the surface) of all DT points that are in touch with it are found first.

The normal force vector (F_{Nsk}) on the kth barrier surface can then be expressed as

$$F_{Nsk} = n_k k_v \int \delta[1 + c_i \dot{\delta}^{m_i}] dA_{sk} \quad (3)$$

where n_k is the unit outward normal vector to the kth barrier surface. Also, the total friction force vector (F_{fsk}) on the kth

surface is given by

$$= -\mu_B k_v \int \delta[1 + c_v\dot{\delta}^{n_v}] \frac{v_{tk}}{|v_{tk}|} dA_{sk} \quad (4)$$

μ_B is the friction coefficient between the barrier and vehicle and v_{tk} is the tangential velocity (to the barrier) vector of each vehicle point in touch with the kth surface.

combining Equations 3 and 4, the total force vector (F_{sk}) kth barrier surface can be expressed as

$$= k_v \int \delta[1 + c_v\dot{\delta}^{n_v}] \left[n_k - \mu_B \frac{v_{tk}}{|v_{tk}|}\right] dA_{sk} \quad (5)$$

total moment vector (M_{sk}) acting at the vehicle center gravity due to force F_{sk} is given by

$$= k_v \int r_{sk} \times \delta[1 + c_v\dot{\delta}^{n_v}] \left[n_k - \mu_B \frac{v_{tk}}{|v_{tk}|}\right] dA_{sk} \quad (6)$$

r_{sk} is the position vector of each vehicle point in touch the kth barrier surface.

evaluating the integrals in Equations 5 and 6, the deformation (δ) is known only at DT points, even though the formation rate and the rest of the variables can be found any vehicle point touching the surface. These DT points scattered over the interface; therefore, a curved surface to be fitted to the values of the integrand at these scattered points to perform the integrations. The volume under this face is then the value of the integral. A review of methods fitting surfaces to scattered data (*4*) indicated that the best thod for the problem in hand is triangularization of the nts. An efficient computer code performing the triangulation was found in a doctoral dissertation by Renka (*5*). code first triangulates the data point locations and then the volume under a linear piecewise surface, or a cubic surface, fitted on any set of data values at the points. integrals over each barrier surface interface found are med to find the total forces and moments.

STRUCTURAL HARD POINTS

The existing HVOSM mathematical model shown in Figure was intended to simulate a sheet metal crush of moderate netration. However, in large angle impacts, stiff automobile uctural components (hard points) slam into the barrier and nerate high impact forces (*6*). To account for these high pact forces, the HVOSM sprung-mass-impact model was dified to include a set of three hard points with user-defined sitions and stiffnesses. Deformation of these hard points, pendicular to the wall, creates a normal force between the icle and the wall. The wall friction is not capable of deforming hard points tangential to the barrier, and therefore a tion force is also created as the points move along the ier (*1*).

Several changes were made during the course of this research the structural hard points of the HVOSM to better simulate acts with rigid barriers. In an angular impact with a rigid ier, the most significant generation of high impact forces e due to the contact of front and rear vehicle axles slamming into the barrier. Therefore, it was assumed that the user always defines the initial position of the hard points to be at the end of an axle. The hard points numbered 1, 2, and 3 should be at the right front, right rear, and left front axle ends, respectively. In an impact with a CSSB, the first point that comes into contact with the barrier is the bottom point of the wheel rim. However, in a wall impact, the midpoint of the rim can be assumed to come into contact first.

Since the axle deformation will probably occur along its longitudinal axis, the hard point is assumed to deform parallel to the longitudinal axis of the axle. If the axle is solid, it can rotate around its roll center. However, since the axle roll angle usually is small, the deformation of the hard point is in the direction of the axle when its roll angle is zero. As the wheel moves up and down due to suspension deflections or to rolling of the axle (if solid), the hard point is also considered to change its position, vertically up or down, in the vehicle-fixed frame by an amount equal to the wheel center vertical displacement.

Force between the vehicle and the barrier at a hard point due to its deformation is assumed to have components both normal and tangential to the barrier surface. The tangential component (F_{ht}) is equal to the normal component (F_{hn}) times the coefficient of friction (μ_B):

$$F_{ht} = \mu_B F_{hn} \quad (7)$$

When resolved in the direction of deformation, these two forces produce the force (F_h) required to deform the hard point, which depends both on the deformation and the deformation rate of the hard point. Hence,

$$F_h = F_{hn} \cos \alpha_n + F_{ht} \cos \alpha_t \quad (8)$$

where α_n is the angle between force F_h and force F_{hn}, which acts normal to the barrier surface, and α_t is the angle between force F_h and force F_{ht} (see Figure 5), which acts in the direction opposite to the velocity of the hard point tangential to the barrier surface. It should be noted that α_n and α_t may not add up to 90°, depending on vehicle orientation.

The model used for the force required to deform the hard point is similar to the model used to find the force intensity at a general point on the vehicle surface. According to this model, force F_h can be expressed as

$$F_h = k_{st}\delta_h[1 + c_{st}\dot{\delta}_h^{n_{st}}] \quad (9)$$

where

k_{st}, c_{st}, and n_{st} = constant parameters for the hard point,
δ_h = total deformation of the hard point, and
$\dot{\delta}_h$ = deformation rate of the hard point.

The constant k_{st} has the dimensions of stiffness (force per unit length), whereas c_{st} and n_{st} are dimensionless.

By equating the right-hand sides of Equations 8 and 9, and then substituting for F_{ht} from Equation 9, and finally solving for F_{hn},

$$F_{hn} = \frac{k_{st}\delta_h[1 + c_{st}\dot{\delta}_h^{n_{st}}]}{[\cos\alpha_n + \mu_B \cos\alpha_t]} \quad (10)$$

The other component of force F_{ht} is found by Equation 7.

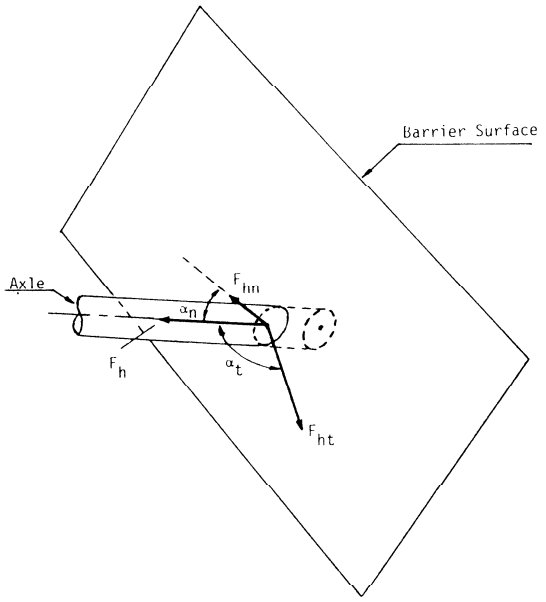

FIGURE 5 Schematic of the determination of forces at a structural hard point in contact with a barrier surface.

IMPROVED SPRUNG-MASS-IMPACT ALGORITIIM

The initial coordinates of the DT points are calculated by the program itself according to user-specified spacings. If the sprung-mass-impact input data are supplied, the initial coordinates of the DT points on the top and bottom vehicle surfaces are calculated at the beginning of the program. Then, for each time step, the corner of the vehicle closest to the barrier is found and checked for contact with the barrier. Once that corner comes into contact, the points are placed on the surfaces on either side of the corner. During the impact, if the vehicle spins and another corner starts crushing against the barrier, then the sides of that corner are checked and, if their points are not placed, those points are defined.

A selected number of DT points on each original surface adjacent to the crushing corner of the vehicle are checked during each time step to see if contact has been made with a barrier surface. The order in which the points are placed on the vehicle makes it possible to be certain that any other points cannot be in contact with the considered barrier surface. Once a point is in contact, then that point is considered to stay in contact until subsequent checks determine that the point has left the surface or has slipped on to another surface. Therefore, it is not checked for contact with any other surface during its stay with the original surface. At each time step, any new points that have come into contact with each surface are collected, and the points that have left each surface are rejected. Then, the deformation undergone during a time step by each point in contact with a barrier surface and the new coordinates of each of these deformed points are calculated.

The coordinates of the corner points of each vehicle/barrier interface area are found to help determine the regions of integration for Equations 5 and 6. Then, all the DT points on the interface and the zero deformation corner points (where the function for the surface to be fitted is known) are triangulated. Some of the corner points that are formed by the intersection of a partially deformed vehicle surface with a barrier surface have unknown deformations. Therefore, a cubic spline is fitted to the known data values to extrapolate the values of the function at these corners with unknown deformations. These corner points then are also added to triangulation, and, finally, the volume under the linear piecewise surface fitted to the data values scattered over the interface is evaluated.

OTHER MODIFICATIONS

Several modifications to the subroutines, other than the sprung-mass-impact routine of the HVOSM, were performed during this research. These changes were made to improve the model's accuracy and involved the models for shock absorbers and tires. Since these modifications are out of the scope of this paper, they are not included. A detailed description is given by Perera (*3*).

VALIDATION AND CALIBRATION OF THE MODIFIED PROGRAM

Once the computer program was completed, it was validated using a three-step procedure. These steps were

1. Comparison with known solutions,
2. Simulation of full-scale crash tests with a rigid vertical wall, and
3. Simulation of full-scale crash tests with the CSSB.

"Calibration" of the program, which was done along with the second and third steps of the validation, involved adjusting the crush properties of the sheet metal and structural hard point properties. Here, the ranges of parameters k_s, c_s, and n_s, estimated using frontal crash tests, were adjusted to better simulate angular crash tests. Initial estimates for parameters k_{sti}, c_{sti}, and n_{sti} were also made and then adjusted to better simulate the selected full-scale crash tests.

In the first step of the validation, the sprung-mass-impact subroutines were used to analyze three selected problems with known solutions. Two of the selected problems have known theoretical solutions and the other an approximate solution. The program was able to produce good approximations of the solutions. A detailed description of these problems, their solutions, and the results of the program is given by Perera (*3*).

Simulation of Full-Scale Crash Tests With a Vertical Wall

Two crash tests, one with a small car (1974 Honda Civic) and the other with a larger car (1975 Plymouth Fury) impacting on a vertical wall instrumented to measure impact forces, were selected for simulation. These were tests 3451-29 and 3451-36, respectively, conducted by the Texas Transportation Institute (TTI) (*7*). In test 3451-29, the Honda Civic was directed

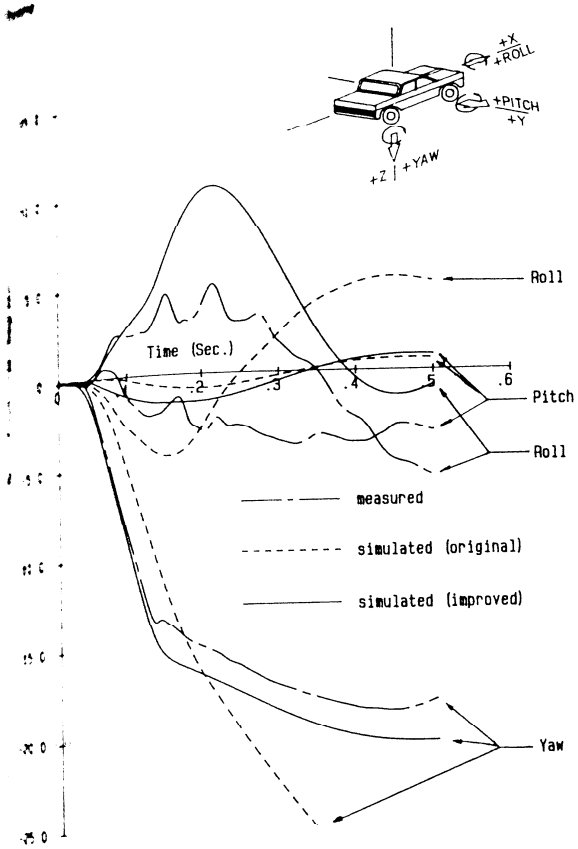

URE 6 Measured and simulated vehicle angular placements for test 3451-29 (1974 Honda Civic on an strumented wall).

at the wall with a speed of 59.0 mph and an angle of 15.5°. The Plymouth Fury in test 3451-36 had an impact speed of 59.8 mph and an impact angle of 24.0°.

Measured and simulated angular vehicle displacements from the test with the Honda Civic are shown in Figure 6. The curves obtained by the unmodified HVOSM program were plotted, along with the simulations by the improved program, to show the improvement due to the new vehicle/barrier crush model. The improved model produced excellent correlation for the yaw displacement. The roll and pitch displacement curves show a slight deviation, but the basic shapes appear to be the same as the measured curves. The primary forces affecting vehicle yaw are the forces due to the crush of the vehicle body. However, the roll and pitch displacements are affected more by the tire and suspension forces. Even though the routines in the HVOSM for tire and suspensions were improved, deviations in roll and pitch can still be expected due to the tire scrubbing on the wall, suspension jams, and unknown suspension damping behavior at high suspension velocities. These limitations are discussed in detail in the following section.

Figure 7 shows measured and predicted lateral wall forces from the test with the Honda Civic. The measured curve and improved simulation show two large peaks corresponding to the impacts of the front and rear corners of the vehicle. The average magnitude and the time of separation of the curve's peaks predicted by the improved model also compare well with the measured curve.

The simulated angular vehicle displacements for the test with the Plymouth Fury are plotted along with the measured curves in Figure 8. The basic shapes of the curves for the improved simulation are the same as the measured curves. Measured and simulated lateral wall forces are shown in Figure 9. Again, the measured and improved simulation curves

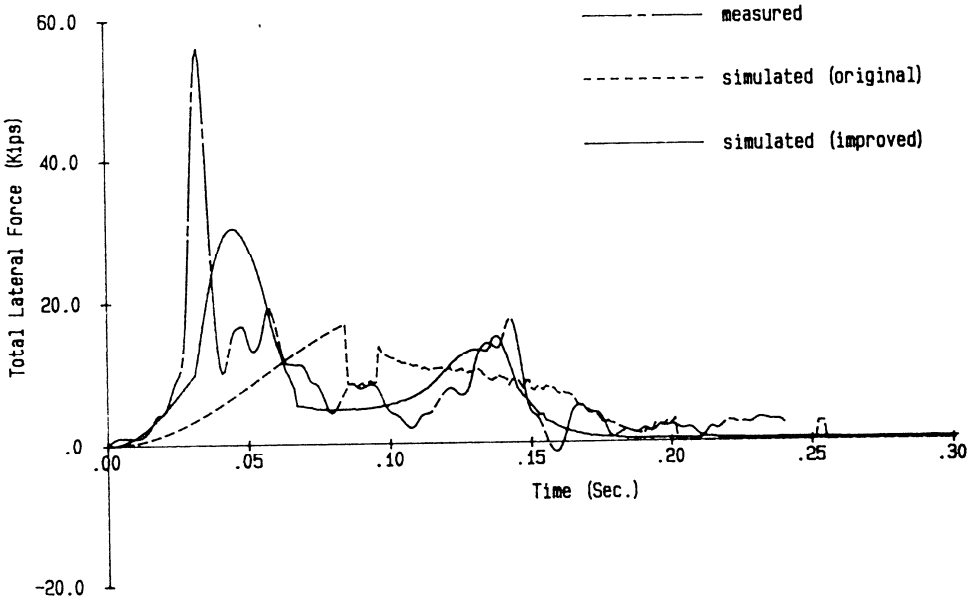

FIGURE 7 Measured and simulated total lateral force on wall for test 3451-29 (1974 Honda Civic).

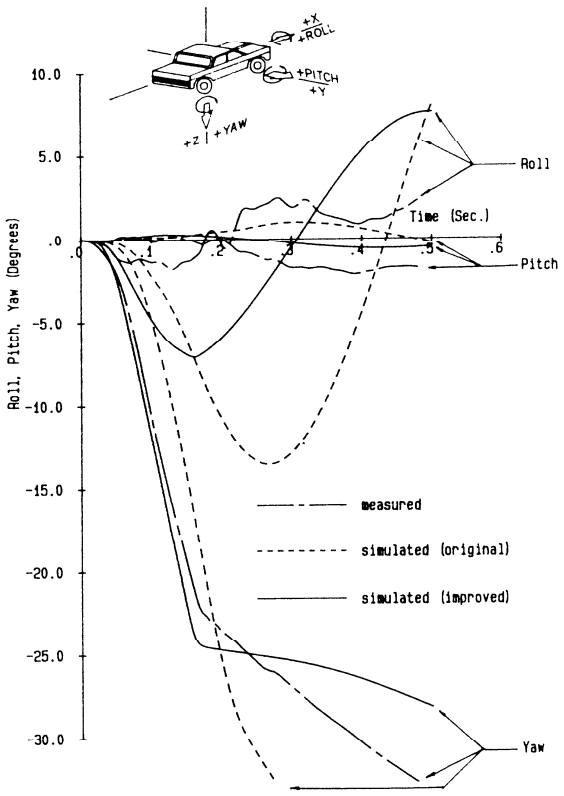

FIGURE 8 Measured and simulated vehicle angular displacements for test 3451-36 (1975 Plymouth Fury on an instrumented wall).

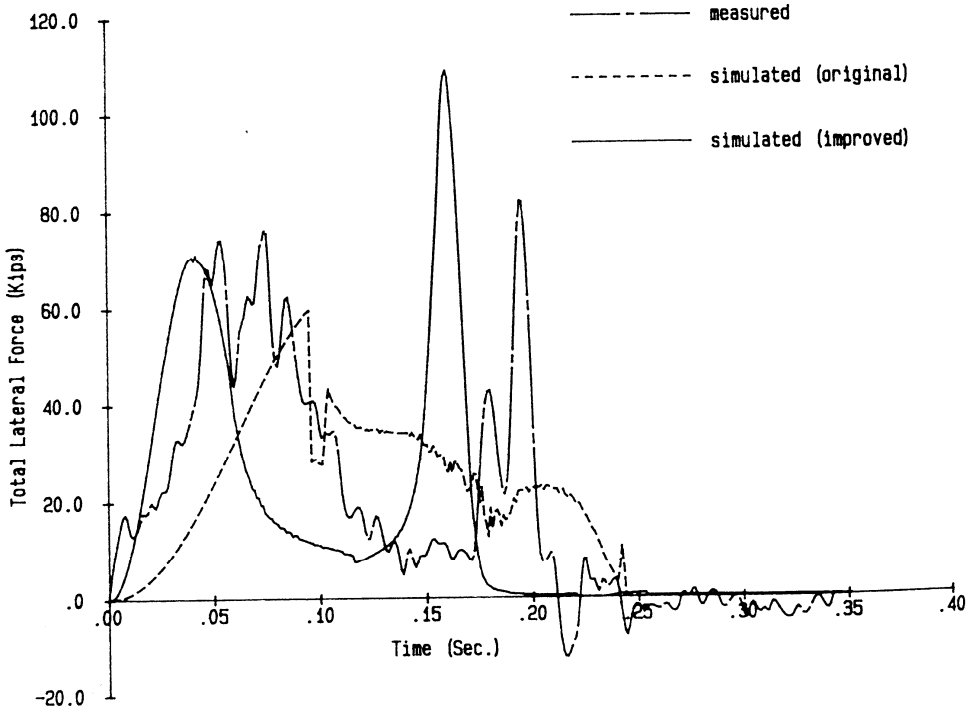

FIGURE 9 Measured and simulated total lateral force on wall for test 3451-36 (1975 Plymouth Fury).

TABLE 1 COMPARISON OF MEASURED AND PREDICTED MAXIMUM 50-MSEC AVERAGE LONGITUDINAL, LATERAL, AND VERTICAL ACCELERATIONS OF THE VEHICLE IN FULL-SCALE CRASH TESTS

Test	Longitudinal Acceleration (G-units)		Lateral Acceleration (G-units)		Vertical Acceleration (G-units)	
	measured	predicted	measured	predicted	measured	predicted
3451-29 (Honda Civic on Wall)	-4.0	-4.0	-10.2	-8.7	1.2	0.3
3451-36 (Plymouth Fury on Wall)	-9.1	-6.2	-15.4	-10.8	2.3	0.2
4798-1 (Honda Civic on CSSB)	-4.6	-2.6	-10.0	-7.4	-3.0	-3.3
4798-3 (Plymouth Fury on CSSB)	-4.2	-3.1	-7.9	-7.3	-1.8	-0.8
7043-1 (Fiat-Uno on CSSB at 15 Deg.)	-4.2	-1.9	-9.0	-6.3	-4.5	-3.6
7043-2 (Fiat-Uno on CSSB at 21.9 Deg.)	-7.1	-5.7	-13.8	-12.2	-4.5	-4.8
7043-3 (Daihatsu Domino on CSSB)	-6.0	-2.9	-7.4	-5.8	-3.6	-2.7
7043-4 (Ford Fiesta on CSSB)	-4.5	-2.3	-7.6	-6.3	-3.7	-5.1
7043-12 (Chevrolet Sprint on CSSB)	-6.0	-4.3	-12.1	-10.0	-4.0	-4.6

Note: 1 G-unit = 32.2 ft/s^2

...e the same general shape, and the front and rear corner ... magnitudes compare well. However, the time at which ... peaks occur shows a deviation.

Measured maximum 50-msec average longitudinal, lateral, ... vertical accelerations for both wall tests are compared in ... 1 with predictions by the improved HVOSM. The sim... underpredicted the maximum accelerations.

...ulation of Full-Scale Crash Tests With CSSB

...en full-scale crash tests with the CSSB were simulated by ... modified HVOSM program in this final phase of the val... and calibration process. An unmodified HVOSM pro... cannot be used for CSSB simulation due to the vertical ... assumption. The first two tests were 4798-1 and 4798-3 ...ducted by TTI (*8*). Test vehicles were similar to those used ... the two instrumented wall tests. These two tests were sim... to further calibrate the vehicle crush and structural ... point parameters. The remaining five tests simulated ...ved micro-size vehicles. These were tests 7043-1 through ... 7043-12 performed by TTI (*9*). Impact conditions for ... these tests are listed in Table 2.

Measured and predicted angular displacements for each test ... shown in Figures 10 through 16. The simulations accu... reproduced the yaw displacement, as in the instru... wall tests. The maximum deviations between the measured and predicted roll curves were about 15°, while the pitch curves were about 18°. However, the general shapes of the predicted roll and pitch curves were similar to those of the measured curves. The deviations are believed to be caused by the limitations in the HVOSM tire and suspension models discussed in the following section.

Measured and predicted longitudinal, lateral, and vertical accelerations for tests 7043-1 through 4 and 7043-12 are shown in Figures 17 through 21. The curves would compare reasonably well if the measured curves were averaged to eliminate the spikes caused by high-frequency vibration of the vehicular structural elements.

Measured and predicted maximum 50-msec average longitudinal, lateral, and vertical accelerations of the vehicle for all seven tests on the CSSB are compared in Table 1. The measured and predicted maximum values compare reasonably well; however, the simulations generally underpredicted the accelerations, as observed in the vertical wall tests. Actual accelerations have perturbations due to the nonhomogeneous structure of the vehicle and high-frequency vibrations of vehicular structural elements. The assumption of a homogeneous crush model results in a smooth acceleration-versus-time curve. These differences in the idealized versus actual vehicle structure is believed to cause the differences in the average accelerations compared over a small time increment. As reported, gross motions and accelerations compared well.

As mentioned previously, the ranges of crush parameters

TABLE 2 IMPACT CONDITIONS OF THE SIMULATED FULL-SCALE CRASH TESTS WITH THE CSSB

Test No.	Test Vehicle	Weight (lb)	Impact Conditions	
			Angle (Deg.)	Speed (mph)
4798-1	1977 Honda Civic	1800	14.5	59.9
4798-3	1977 Plymouth Fury	4500	16.5	58.6
7043-1	1985 Fiat Uno-45	1560	15.0	58.4
7043-2	1985 Fiat Uno-45	1560	21.9	61.6
7043-3	1985 Daihatsu Domino	1280	16.0	60.0
7043-4	1985 Ford Fiesta	1530	16.0	61.6
7043-12	1985 Chevy Sprint	1610	20.1	61.6

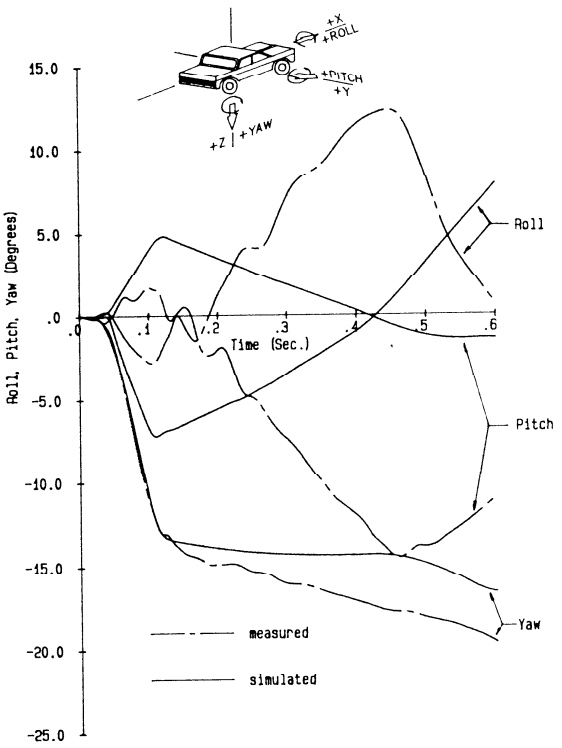

FIGURE 10 Measured and simulated vehicle angular displacements for test 4798-1 (1977 Honda Civic on a CSSB).

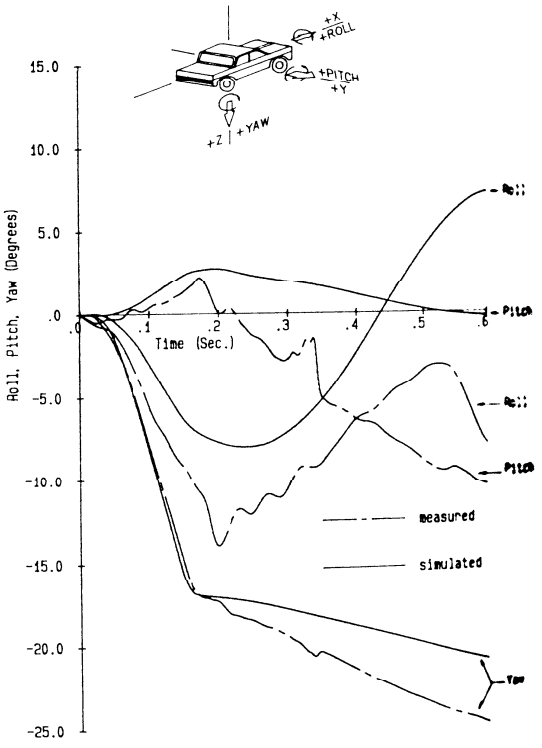

FIGURE 11 Measured and simulated vehicle angular displacements for test 4798-3 (1977 Plymouth Fury on a CSSB).

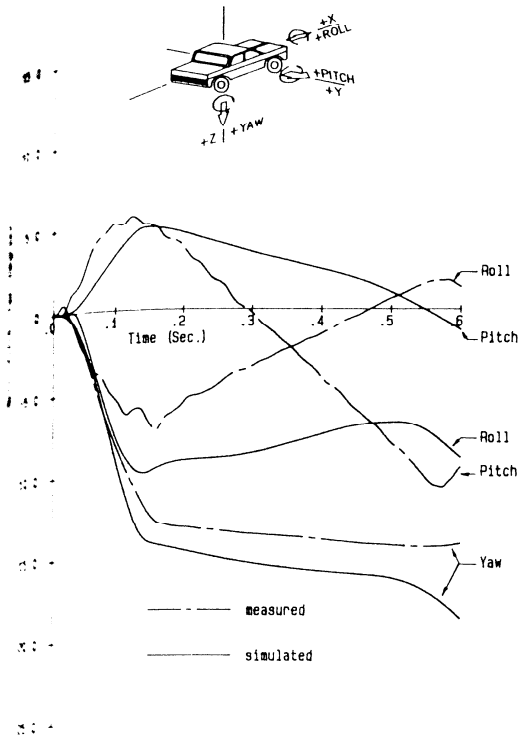

FIGURE 12 Measured and simulated vehicle angular displacements for test 7043-1 (1985 Fiat Uno-45 on a CSSB at 15°).

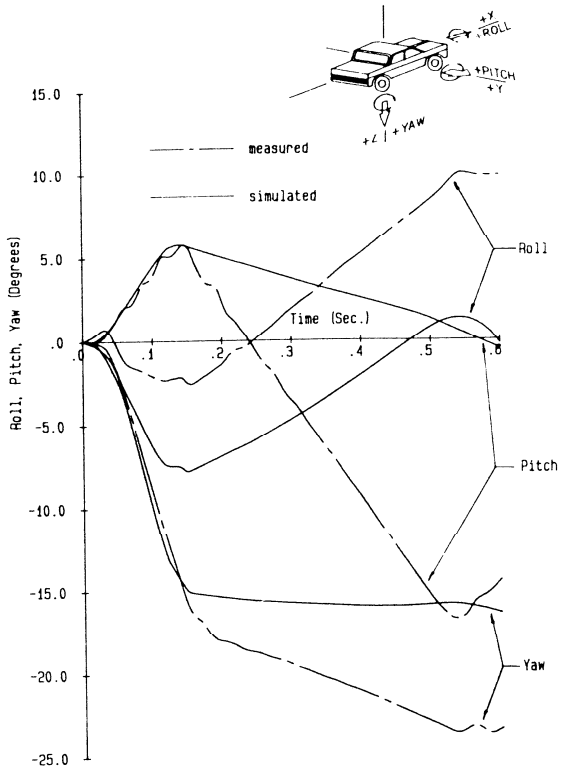

FIGURE 14 Measured and simulated vehicle angular displacements for test 7043-3 (1985 Daihatsu Domino on a CSSB).

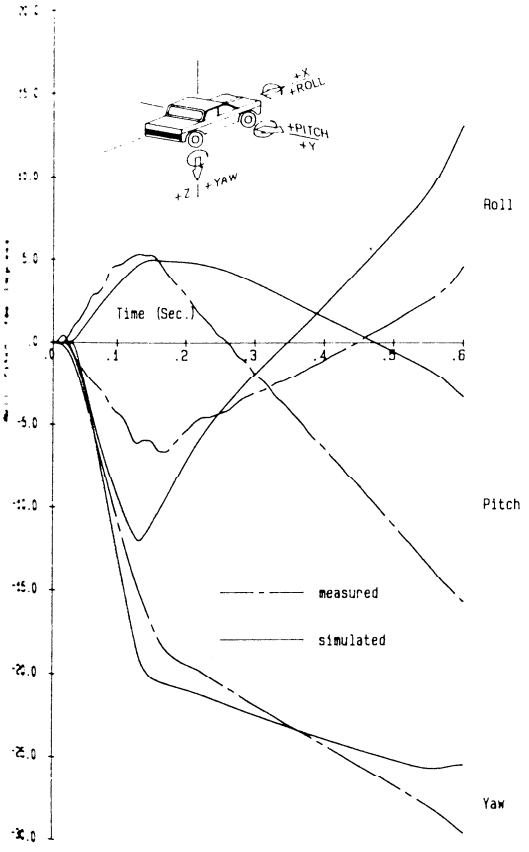

FIGURE 13 Measured and simulated vehicle angular displacements for test 7043-2 (1985 Fiat Uno-45 on a CSSB at 21.9°).

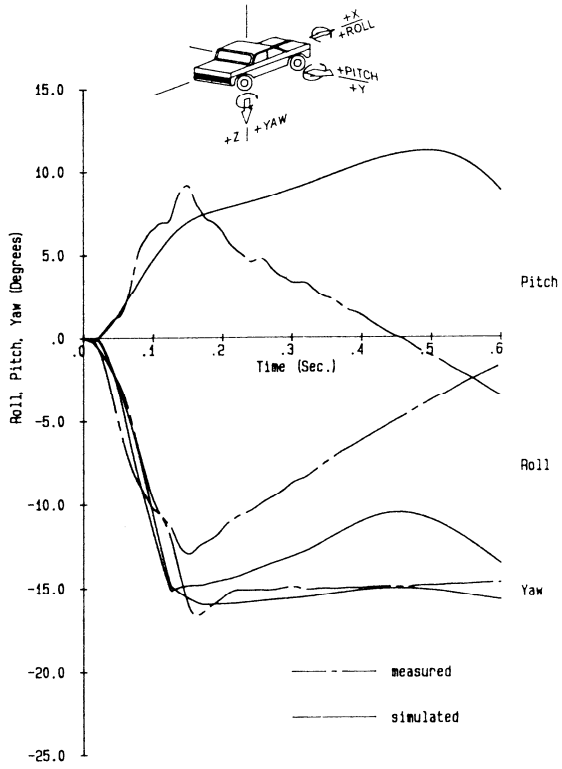

FIGURE 15 Measured and simulated vehicle angular displacements for test 7043-4 (1985 Ford Fiesta on a CSSB).

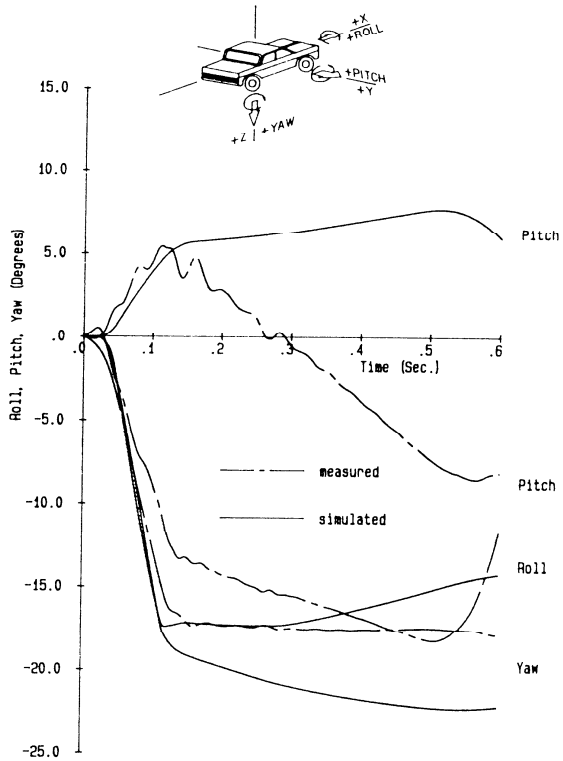

FIGURE 16 Measured and simulated vehicle angular displacements for test 7043-12 (1985 Chevrolet Sprint on a CSSB).

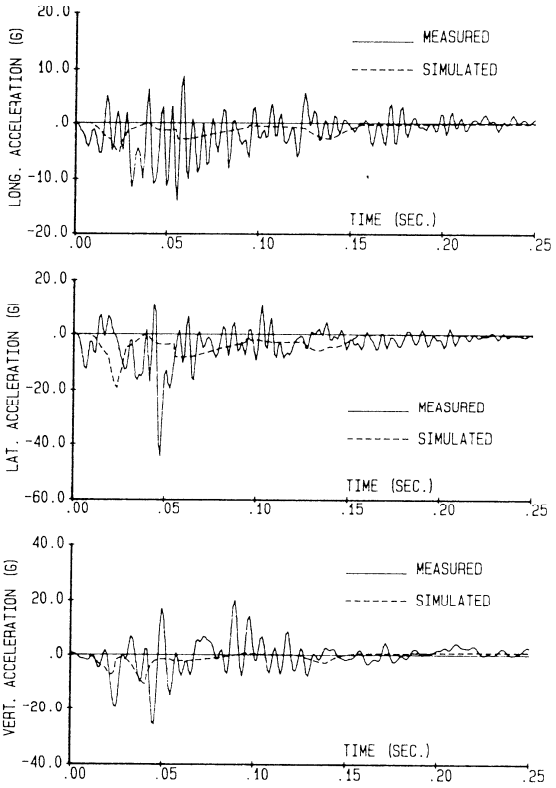

FIGURE 17 Measured and simulated longitudinal, lateral, and vertical accelerations for test 7043-1 (1985 Fiat Uno-45 on a CSSB at 15°).

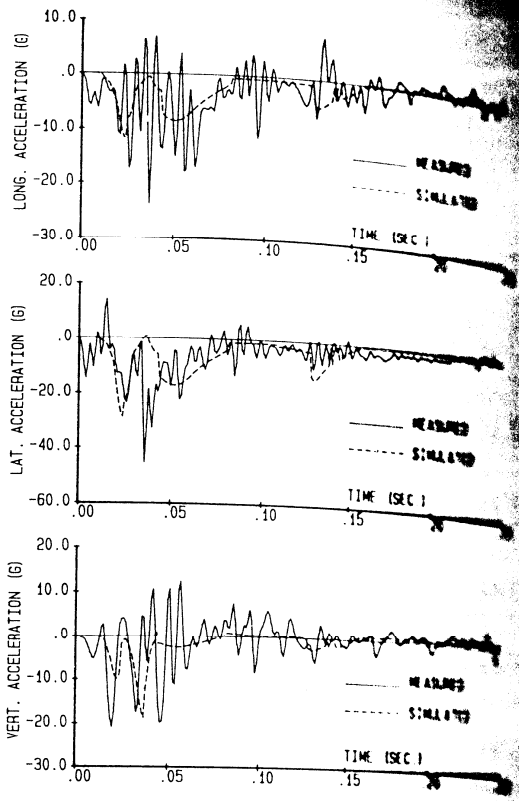

FIGURE 18 Measured and simulated longitudinal, lateral, and vertical accelerations for test 7043-2 (1985 Fiat Uno-45 on a CSSB at 21.9°).

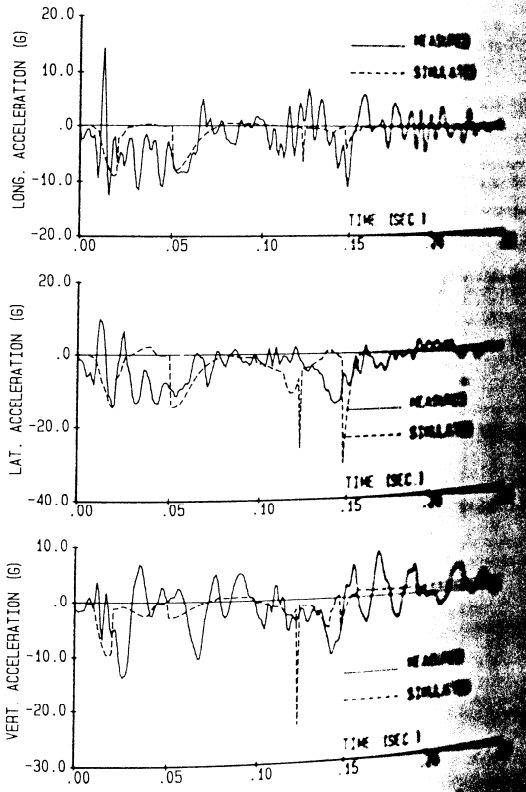

FIGURE 19 Measured and simulated longitudinal, lateral, and vertical accelerations for test 7043-3 (1985 Daihatsu Domino on a CSSB).

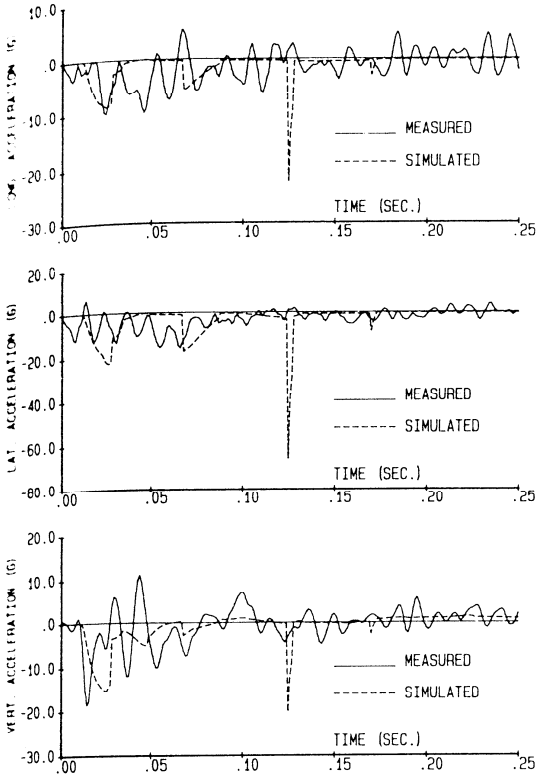

FIGURE 20 Measured and simulated longitudinal, lateral, and vertical accelerations for test 7043-4 (1985 Ford Fiesta on a CSSB).

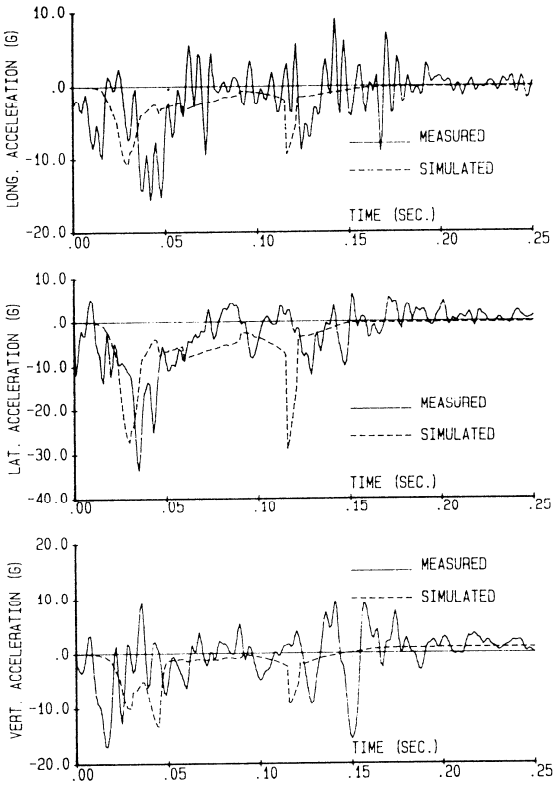

FIGURE 21 Measured and simulated longitudinal, lateral, and vertical accelerations for test 7043-12 (1985 Chevrolet Sprint on a CSSB).

c_1, c_3, and n_3 estimated in frontal impact simulations were adjusted for angular impacts during the validation and calibration procedure described above. The values of these parameters used for each different vehicle were adjusted within the basic range to better simulate each test and are listed in Table 3. The stiffness value used for the rear structural hard point was higher than that for the front, to account for the differences in the front and rear suspension system. All of these values are tabulated in Table 4.

As stated, a relationship between crush parameters k_1, c_1, and n_1 and the vehicle mass could not be found. However, the inclusion of vehicles with weights of 4,500 lb and 1,800 lb in the crush parameter tables covers the *NCHRP Report 350* (*10*) requirements for barrier evaluation. The rest of the vehicles will be useful in case of any changes in safety criteria due to the trend towards small vehicles.

LIMITATIONS OF THE IMPROVED HVOSM PROGRAM

During rigid barrier impact, the leading tire and associated suspension system is typically subjected to high loads and loading rates, resulting in large displacements and usually structural failure in the form of bent rims and a wheel jammed in and back from its normal position. Little data are available on tire and suspension system damping properties for high loading rates. The models simply are not designed to simulate structural failures.

Certain assumptions were necessary to simulate tire-barrier interaction because of extraneous and excessively large tire forces that occur in the HVOSM during shallow angle impacts with steep barrier faces. These unreasonably high values result from the limitations of the thin disk tire model (*9*). To eliminate this problem, the near vertical upper slope of the barrier cross section was removed from the tire contact region (or the curb as referred to in the HVOSM documentation). However, the structural hard point locations and stiffness values were properly selected to prevent the wheels from penetrating the removed upper slope.

CONCLUSIONS

Simulations of the full-scale crash tests by the improved HVOSM correlated well with the measured results, and angular orientation of the vehicle with time was a primary response. Predicted yaw rotations compared well with measured values. Deviations up to about 15° in roll rotations and about 18° in pitch rotations were observed. However, the general shapes of predicted roll and pitch curves compared well with the measured curves. The measured and predicted acceleration data compared reasonably well in all tests. However, a tendency to underpredict the maximum 50-msec average accelerations was noted. The primary forces affecting the yaw rotations are vehicle crush forces, while the roll and pitch rotations are equally affected by tire and suspension forces. Achieving excellent correlation between predicted and measured yaw

TABLE 3 VEHICLE CRUSH PARAMETERS USED IN CSSB SIMULATIONS

Vehicle	k_v (lb./in.^{3})	c_v	n_v
1974 Honda Civic	0.85	0.1	0.6
1975 Plymouth Fury	1.0	0.3	0.6
1985 Fiat Uno-45	0.7	0.15	0.6
1985 Daihatsu Domino	0.5	0.05	0.5
1985 Ford Fiesta	0.65	0.05	0.5
1985 Chevrolet Sprint	0.9	0.3	0.6

TABLE 4 STRUCTURAL HARD POINT PARAMETERS USED IN CSSB SIMULATIONS

Vehicle	Front			Rear		
	k_{sti} (lb/in)	c_{sti}	n_{sti}	k_{sti} (lb/in)	c_{sti}	n_{sti}
1974 Honda Civic	500	0.2	0.8	700	0.4	1.0
1975 Plymouth Fury	400	0.2	0.6	1000	0.35	0.75
1985 Fiat Uno-45	500	0.2	0.7	600	0.3	0.8
1985 Daihatsu Domino	500	0.3	0.9	600	0.45	1.0
1985 Ford Fiesta	600	0.3	0.8	700	0.4	0.9
1985 Chevrolet Sprint	400	0.2	0.6	500	0.3	0.8

rotations is indicative of a reliable vehicle sheet metal model. Limitations in HVOSM tire and suspension models lead to deviations in roll and pitch rotations. These limitations notwithstanding, the improved HVOSM program is a useful tool, when properly calibrated, in the analysis of barrier and vehicle parameters as they affect impact performance.

ACKNOWLEDGMENTS

This research study was funded by NCHRP and FHWA. The author would like to thank Hayes E. Ross, Jr., for his guidance and encouragement as advisory committee chairman. The support and helpful suggestions of other committee members—J. T. Tielking, R. W. James, D. W. Childs, and L. L. Schumaker—are also acknowledged. Special thanks are extended to Dean L. Sicking for his encouragement and helpful discussions.

REFERENCES

1. D. J. Segal. *Highway-Vehicle-Object-Simulation Model 1976.* Reports FHWA-RD-75-162–165. Calspan Corporation, Buffalo, N.Y., 1976.
2. R. R. McHenry, D. J. Segal, and N. J. DeLays. *Determination of Physical Criteria for Roadside Energy Compression Systems.* Technical Report Cal-VJ-2251-V-1. Cornell Aeronautical Laboratory, Inc., Buffalo, N.Y., 1967.
3. H. S. Perera. *Simulation of Vehicular Impacts with Safety Shaped Barrier.* Ph.D. dissertation. Department of Civil Engineering, Texas A&M University, College Station, 1987.
4. L. L. Schumaker. Fitting Surfaces to Scattered Data. *Approximation Theory II. Symposium on Approximation Theory.* University of Texas, Austin, 1976.
5. J. R. Renka. *Triangulation of Bivariate Interpolation for Irregularly Distributed Data Points.* Ph.D. dissertation. Department of Mathematics, University of Texas, Austin, 1981.
6. R. D. Young, E. R. Post, H. E. Ross, and R. M. Holcomb. *Simulation of Vehicle Impact with the Texas Concrete Median Barrier. Volume I: Test Comparisons and Parameter Study.* Research Report 140-5. Texas Transportation Institute, Texas A&M University, College Station, 1972.
7. C. E. Buth, A. Arnold, W. L. Campise, T. J. Hirsch, D. L. Ivey, and J. S. Noel. *Safer Bridge Railings.* Report FHWA-RD-82-074.2, Vol. 4, App. C, Part 2. FHWA, U.S. Department of Transportation, 1984.
8. W. L. Campise and C. E. Buth. *Performance Limits of Longitudinal Barrier Systems*, Vol. III, App. B. FHWA, U.S. Department of Transportation, 1985.
9. H. E. Ross, H. S. Perera, D. L. Sicking, and R. P. Bligh. *NCHRP Project 22-6: Roadside Safety Design for Small Vehicles*, Vol. II. TRB, National Research Council, Washington, D.C., 1988.
10. *NCHRP Report 230: Recommended Procedures for the Safety Performance Evaluation of Highway Appurtenances.* TRB, National Research Council, Washington, D.C., 1981.

Publication of this paper sponsored by Committee on Roadside Safety Features.